Simulation of Cycle-to-Cycle Instabilities in SiO_x-Based ReRAM Devices Using a Self-Correlated Process with Long-Term Variation

E. Miranda, *SM, IEEE,* A. Mehonic, W. H. Ng, *M, IEEE,* A. J. Kenyon, *SM, IEEE*

***Abstract*—Cycle-to-cycle (C2C) current variability occurring in ReRAM devices is not only an stochastic feature inherent to electron transport in low dimensional conducting structures but also a consequence of the measurement protocol used to characterize the device evolution during resistance switching. In such latest case, C2C changes depend on the particular arrangement of the ions or vacancies that form the conducting filament spanning the dielectric film. In this work a discrete first order autoregressive model AR(1) with long-term variation is used to represent both the random and the "deterministic" behaviors of the high resistance state current. Simulation of C2C instabilities in SiO_x is carried out through the quantum point-contact model for filamentary electron transport in dielectrics with fluctuating confinement potential barrier height. Simplicity is of utmost importance since the proposed approach is aimed for circuit simulation environments in which complex and time-consuming computations need to be avoided.**

***Index Terms*—Resistive Switching, Variability, MIM, SiO_x**

I. Introduction

ReRAM (Redox-based Resistive RAM) devices are considered one of the most promising candidates to overcome the limitations of conventional memory devices such as Flash, particularly in connection with scalability issues [1]. Electron transport in ReRAMs is single or multi filamentary-type with metal atoms or oxygen vacancies forming conducting pathways spanning an oxide layer [2]. These pathways can grow and dissolve reversibly by applying voltage pulses or sweeps with the appropriate polarity. Transitions to the low (LRS) and to the high (HRS) resistance state are referred to as the SET and RESET processes, respectively. While LRS is often ascribed to Ohmic conduction, HRS has been related to a wide variety of mechanisms including Schottky and Poole-Frenkel emission, trap assisted tunnelling, space charge limited, and quantum point-contact (QPC) conduction [2-5]. In this latest case, the filamentary structure is treated like a quantum wire with a confinement potential barrier located at its narrowest section [6]. The QPC model is able to explain linear and nonlinear quantization effects observed in ReRAMs [7-18]. Due to its low dimensional nature, the HRS conducting filament (CF) is prone to suffer microstructural changes [19-23] that appear as current fluctuations around a central trend represented by an effective confinement barrier [18]. This barrier changes from C2C since atomic arrangements are not identical after each SET and RESET event. The way the barrier changes is also largely influenced by the measurement protocol used to characterize the switching capability of the device. The existence of a central tendency with spread for the current modification is consistent with the idea of a conductive region formed by a bunch of electron transport channels with randomly changing transmission properties [8,18].

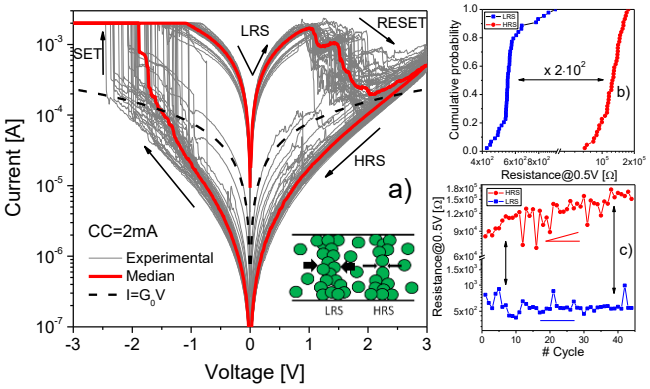

Fig.1: a) Experimental *I-V* characteristics for the devices investigated in this letter. The inset shows the classical interpretation of LRS and HRS in terms of the lateral size of the constriction. The red solid line is the median curve. The dashed line corresponds to the conduction characteristic of a monomode ballistic conductor. G_0 is the quantum conductance unit. b) Resistance window for LRS and HRS measured at 0.5V. c) Evolution of the resistance window.

In this Letter, a stochastic model for the electron transport characteristic in Si-rich silica (SiO_x) filamentary-type switches compatible with previous observations of quantization effects [8] is reported. The proposed approach deals with variability using an autoregressive (AR) model with a long-term trend for the confinement barrier height. This formulation is useful for circuit simulation environments where complex and time-consuming computations like those based on 3D kinetic Monte Carlo techniques are not allowed [24-26]. The attention here is exclusively focused on HRS since this low state current corresponds to the more unstable and more difficult to control characteristic in ReRAM devices.

E. Miranda is with the Departament d'Enginyeria Electrònica, Universitat Autònoma de Barcelona, 08193 Barcelona, Spain (e-mail: enrique.miranda@uab.cat). A. Mehonic, W. Ng, and A.J. Kenyon are with the Department of Electronic & Electrical Engineering, UCL, London, UK. EM and AJK acknowledge financial support from the Leverhulme Trust, UK. AM acknowledges financial support from the Royal Academy of Engineering. EM acknowledges support from MINECO, Spain (TEC2017-84321-C4-4-R).

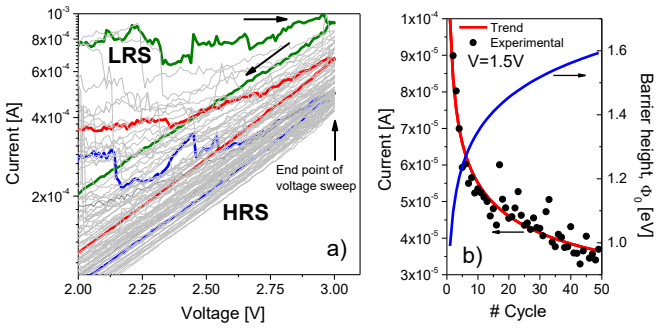

Fig.2: a) Detail of the RESET region in Fig.1.a. Some selected curves are shown with heavy solid lines. b) Current trend and evolution of the confinement barrier height as a function of the cycle number. Symbols are experimental data.

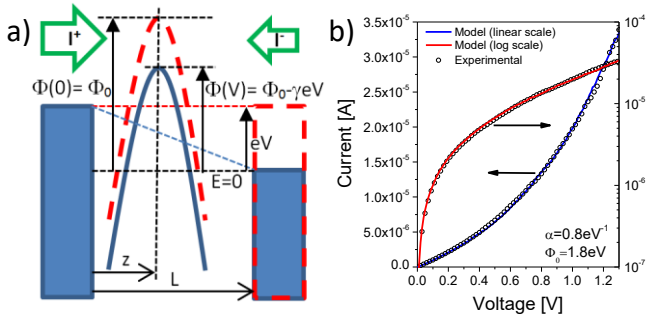

Fig.3: a) Schematic of the confinement barrier profile and effect of the applied voltage. b) Typical experimental and model results using expression (3).

II. Experimental Characterization

ReRAM devices were fabricated on Si substrates with a top layer of 4 µm of thermal SiO_2. 280 nm of Mo (bottom electrode) was deposited onto the SiO_2 layer by sputtering. The switching oxide was deposited by reactive magnetron sputtering, in which an undoped Si target was used to sputter the SiO_x thin film (35 nm) onto the substrate in an O-rich environment. After this, a thin (3 nm) adhesion layer of Ti followed by a 115 nm layer of Au was deposited by e-beam evaporation to serve as top electrode (400 µm × 400 µm). The devices were initially electroformed with a maximum voltage ramp of -3 V and a current compliance CC=2 mA [27]. After this, the devices were subjected to successive voltage sweeps: 0V→-3V→3V→0V. The *I-V* characteristics are illustrated in Fig.1.a. During the sweep back to 0 V, the HRS curves show spontaneous instabilities which are mostly confined to the conductance region $G<G_0$, $G_0=2e^2/h$ being the quantum-conductance unit. Although Fig.1.b shows a well-defined resistance window (≈10^2@0.5V), Fig.1.c reveals the existence of a trend in HRS that is not captured by the previous plot. The origin of this trend can be understood from the data shown in Fig.2.a, which is a detail of the RESET region in Fig.1.a. Remarkably, the RESET dynamics (right-going arrow in Fig.2.a) and the maximum excursion of the input signal (3V in this case) determine the starting point (left-going arrow) of the corresponding HRS *I-V* characteristic. This indicates that C2C evolution and unstabilities need to be assessed considering the particularities of the measurement protocol.

III. Model Equations and Simulations

Conduction through fully and partially formed CFs can be modeled using an effective confinement barrier of height Φ_0 that takes into account the series and parallel combination of multiple scatterer centers [18]. Because of the atomic rearrangements, the transmission properties of the scatterers are expected to change from C2C leading to a global modification of Φ_0. The current that flows through the device can be calculated using the Landauer formula as [6]:

$$I = \frac{2e}{h}\int_{-\infty}^{+\infty} T(E,V)[f(E-eV)-f(E)]\,dE \qquad (1)$$

where T is a transmission coefficient, f the Fermi-Dirac distribution function, E the energy, V the applied voltage, e the electron charge, and h the Planck's constant. Assuming that the confinement barrier can be approximated at its narrowest section by an inverted parabolic barrier of height $\Phi(V)$, T can be expressed as [3,28]:

$$T(E,V) \approx exp\{\alpha[E-\Phi(V)]\} \qquad (2)$$

where α is a parameter related to the longitudinal barrier profile. Now, for a linear relationship $\Phi(V)=\Phi_0-\gamma eV$ with $\gamma = z/L$ a coupling factor (see Fig. 3.a) [29], from (1) and (2):

$$I = \frac{2e}{\alpha h} exp(-\alpha\Phi_0)\{exp[\alpha e(\gamma+1)V] - exp[\alpha e\gamma V]\} \qquad (3)$$

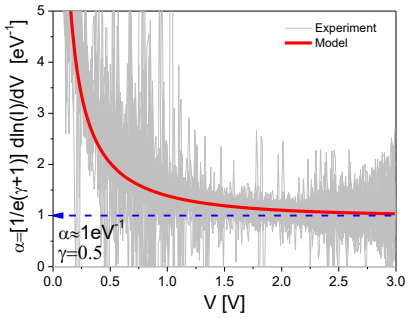

Fig. 4: Experimental (solid lines) and model (heavy solid line) results used to investigate the dependence of the model equation (3) on the parameter α. The arrow indicates the estimated value for α.

(3) is strictly valid for $eV \leq \Phi_0/(1+\gamma)$ in the zero-temperature limit. If for the sake of completeness, a series resistance R_S, common to all conducting channels [30], needs to be included in the above treatment, replacing $V \rightarrow V\text{-}IR_S$ in (3) yields $I \approx I^+ - I^-$ where:

$$I^+ = \frac{1}{\alpha e(\gamma+1)R_S} W\{G_0(\gamma+1)R_S exp[-\alpha(\Phi_0 - e(\gamma+1)V)]\} \qquad (4)$$

$$I^- = \frac{1}{\alpha e\gamma R_S} W\{G_0\gamma R_S exp[-\alpha(\Phi_0 - e\gamma V)]\} \qquad (5)$$

are the right- and left-going current components shown in Fig.3.a. W is the Lambert function. In our case, R_S plays no significant role but can be of relevance in others [31]. Typical fitting results using (3) in linear and log scales are illustrated in Fig.3.b. Figure 2.b reveals that the reduction of the C2C

experimental current at a fixed bias can be accounted for by an increasing confinement barrier height. For the current range under study the proposed model yields reasonable values for Φ_0 but for lower HRS current values, a trap-assisted tunneling model would be more appropriate [32].

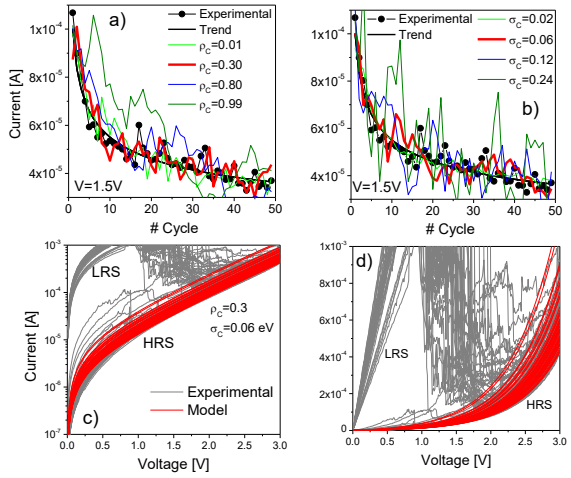

Fig. 5: Effect of a) ρ_C and b) σ_C on the current. Symbols are experimental data. c) Log-linear and d) linear-linear plots: sequence of *I-V* curves generated using (4) and (7). Best fitting results are obtained using ρ_C=0.3 and σ_C=0.06.

In order to assess the role played by α in (3), Fig.4 shows how this parameter can be estimated from data. At the largest biases, α reads:

$$\alpha \approx \frac{1}{e(\gamma+1)} \frac{dln(I)}{dV} \tag{6}$$

which is independent of Φ_0. From experiments, an average value $\alpha \approx 1\text{eV}^{-1}$ for γ=0.5 (constriction's bottleneck located in the middle of the oxide film) is obtained. For the sake of simplicity, α (slope of the *ln*(*I*)-*V* curve) will be considered fixed so that variability will be exclusively ascribed to Φ_0 (see Fig.3.a). In what follows, model results are reported for positive voltages but they equally apply to negative ones because of the symmetry of the HRS curves. C2C variability is simulated as follows: it is assumed that for cycle *i* the barrier height φ_{0i} is expressed as an AR(1) process with trend Φ_{0i}:

$$\varphi_{0i} = (1-\rho_C)\Phi_{0i} + \rho_C \varphi_{0i-1} + \sigma_C \epsilon_i \tag{7}$$

where ρ_C is the self-correlation coefficient, σ_C the standard deviation, and $\epsilon_i \sim N(0,1)$ a Wiener process (white noise). AR processes of higher order can be considered if necessary [33]. Now φ_{0i} replaces Φ_0 in (3). For our experimental conditions:

$$\Phi_{0i} = 0.155 \cdot \ln i + 0.99 \quad [\text{eV}] \tag{8}$$

This particular dependence arises from the linear increase of the HRS resistance with the cycle number shown in Fig.1.a. For a different measurement protocol (for instance, different end voltage or pulse switching condition) the functional dependence in (8) needs to be identified. This relationship can be a function of other parameters (injected charge, pulse amplitude, etc) as well in addition to the cycle number. Importantly, for an AR(1) process, $\varphi_0 \sim N(\Phi_{0i}, \sigma'^2_C)$ where $\sigma'^2_C = \sigma^2_C/(1-\rho^2_C)$ is the effective variance [33]. This result is compatible with the log-normal current fluctuations reported in literature [34]. The effects of ρ_C and σ_C on the HRS current are illustrated in Figs. 5.a-d. As can be seen, the consecutive *I-V* curves follow a trend but are not completely ordered. Physically, the reduction of the current observed in Fig.5 as the cycling experiment proceeds can be explained by an effective confinement barrier increase which in turn can be attributed to a thinning process of the CF. In other words, as the stabilization process evolves, fewer and fewer atomic sites contribute to the current or are able to switch to a higher transmission probability arrangement.

Finally, let us discuss how Eqns. (3) and (7) can be implemented in a generic circuit simulator. Notice that this is not a compact model for ReRAM since it is not aimed to deal with transitions and LRS variability. As shown in Fig. 6, (3) can be modelled as a voltage-driven current generator (I_{QPC}) with a series resistance R_S (eqns. (4) and (5)). The AR process (7) can be simulated using another voltage-driven current generator which includes the trend, the previous barrier height (sampled at V_x) and the gaussian noise (obtained using the Box-Muller transform [35]). The capacitor *C* is used to store the barrier height value as a voltage and must be initiallized with a current sampled from the normal distribution $N(\Phi_{0i}, \sigma'^2_C)$ so as to ensure a process with invariant measure (without transient). R_P is a parallel resistance with value 1Ω. The proposed approach is similar to that used for the memory state of a memristor [36]. The index *i* used to calculate the cycle trend (8) can be defined as a global variable (run number) or can be incorporated into the model script as a discrete ramp.

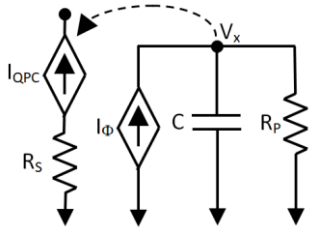

Fig. 6: Schematic of the simulation model. The current generators I_{QPC} and I_Φ represent the filamentary current and the AR process, respectively. Node V_x is used to control the tunneling current. The capacitor *C* stores the information.

IV. Conclusions

An stochastic model for the C2C instabilities in the HRS *I-V* characteristic of SiO_x-based ReRAM devices based on quantum point-contact conduction was presented. The main advantage of our proposal is the simplification of computations in comparison with previous simulation schemes. It is clear that the limitations are also higher but the final result is a tool appropriate for circuit simulators in which the microscopic physical aspects of the electron transport problem are hard or impossible to implement in detail.

REFERENCES

[1] Resistive switching, From fundamentals of nanoioic redox processes to memristive device applications, Wiley-VCH, Eds. D. Ielmini and R. Waser, 2015. ISBN: 978-3-527-33417-9

[2] J. Lee, S. Lee, T. Noh, Resistive switching phenomena: A review of statistical physical approaches, Appl Phys Rev, vol. 2, 031303 (2015). DOI: 10.1063/1.4929512

[3] E. Miranda, C. Walczyk, C. Wenger, T. Schroeder, Model for the resistive switching effect in HfO_2 MIM structures based on the transmission properties of narrow constrictions, IEEE Electron Dev Lett, vol. 31, pp. 609–61 (2010). DOI: 10.1109/LED.2010.2046310

[4] D. Garbin, E. Vianello, Q. Rafhay, M. Azzaz, P. Candelier, B. DeSalvo, G. Ghibaudo, L. Perniola, Resistive memory variability: A simplified trap-assisted tunneling model, Solid St Electron, col. 115, pp. 126-132 (2016). DOI: 10.1016/j.sse.2015.09.004

[5] A. Mehonic, S. Cueff, M. Wojda, S. Hudziak, C. Labbe, R. Rizk, A. J. Kenyon, Electrically tailored resistance switching in silicon oxide, Nanotechnology, vol. 22, pp. 455201, 2012. DOI: 10.1088/0957-4484/23/45/455201

[6] S. Datta, Electronic Transport inMesoscopic Systems. Cambridge, U.K.: Cambridge Univ. Press, 1997. ISBN: 978-0521599436

[7] R. Degraeve, Ph. Roussel, L. Goux, D. Wouters, J. Kittl, L. Altimime, M. Jurczak, G. Groeseneken, Generic learning of TDDB applied for improved understanding of conduction and switching mechanism through multiple filaments, Int Electron Dev Meeting, 28.4.1-28.4.4 2010. DOI**:** 10.1109/IEDM.2010.5703438

[8] A. Mehonic, A. Vrajitoarea, S. Cueff, S. Hudziak, H. Howe, C. Labbé, R. Rizk, M. Pepper, A.J. Kenyon, Quantum conductance in silicon oxide resistive memory devices, Sci Rep, vol. 3, 2708 (2013). DOI:10.1038/srep02708

[9] Y. Syu, T. Chang, J. Lou, T. Tsai, K. Chang, M Tsai, Y. Wang, M. Liu, S. Sze, Atomic-level quantized reaction of HfO_x memristor, App Phys Lett, vol. 102, 172903 (2013). DOI: 10.1063/1.4802821

[10] L. Goux, N. Raghavan, A. Fantini, R. Nigon, S. Strangio, R. Degraeve, G. Kar, Y. Chen, F. De Stefano, V. Afanasev, M. Jurczak, On the bipolar resistive-switching characteristics of Al_2O_3 and HfO_2-based memory cells operated in the soft-breakdown regime, J Appl Phys, vol. 116, 134502 (2014). DOI: 10.1063/1.4896841

[11] Y. Li, S. Long, Y. Liu, C. Hu, J. Teng, Q. Liu, H. Lv, J. Suñé, M. Liu, Conductance quantization in resistive random access memory, Nano Res Lett, 10:420 (2015). DOI: 10.1186/s11671-015-1118-6

[12] H. Lv, X. Xu, P. Sun, H. Liu, Q. Luo, Q. Liu, W. Banerjee, H. Sun, S. Long, L. Li, M. Liu, Atomic view of filament growth in electrochemical memristive elements, Sci Rep, 5:13311 (2015). DOI: 10.1038/srep13311

[13] X. Zhong, I. Rungger, P. Zapol, O. Heinonen, Oxygen modulated quantum conductance for ultra-thin HfO_2-based memristive switching devices, Phys Rev B, vol. 94, 165160 (2016). DOI: 10.1103/PhysRevB.94.165160

[14] S. Oliver, J. Fairfield, A. Bellew, S. Lee, J. Champlain, L. Ruppalt, J. Boland, P. Vora, Quantum point contacts and resistive switching in Ni/NiO nanowire junctions, App Phys Lett, 109, 203101 (2016). DOI: 10.1063/1.4967502

[15] G. Holloway, O. Ivanov, R. Gavrilov, A. Bluschke, B. Hold, J. Baugh, Electric breakdown in thin Si oxide modeled by a quantum point contact network, IEEE Trans Elec Dev, vol. 63, pp. 3005-10 (2016). DOI: 10.1109/TED.2016.2577611

[16] S. Nandakumar, M. Minvielle, S. Nagar, C. Dubourdieu, B. Rajendran, A 250 mV $Cu/SiO_2/W$ memristor with half-integer quantum conductance states, Nano Lett, 16, pp. 1602-08 (2016). DOI: 10.1021/acs.nanolett.5b04296

[17] W. Yi, S. Savelev, G. Medeiros-Ribeiro, F. Miao, M. Zhang, J. Joshua Yang, A. Bratkovsky, R. Stanley Williams, Quantized conductance coincides with state instability and excess noise in tantalum oxide memristors, Nature Comm, vol. 7, 11142 (2016). DOI:10.1038/ncomms11142

[18] E. Miranda, A. Mehonic, J. Suñe, A.J. Kenyon, Multi-channel conduction in redox-based resistive switch modelled using quantum point contact theory, Appl Phys Lett, vol. 103, 222904 (2013). DOI: 10.1063/1.4836935

[19] R. Degraeve, A. Fantini, N. Raghavan, L. Goux, S. Clima, B. Govoreanu, A. Belmonte, D. Linten, M. Jurczak, Causes and consequences of the stochastic aspect of filamentary RRAM, Mic Rel, vol. 147, 171-175 (2015). DOI: 10.1016/j.mee.2015.04.025

[20] G. Piccolboni, G. Molas, D. Garbin, E. Vianello, O. Cueto, C. Cagli, B. Traore, B. De Salvo, G. Ghibaudo, L. Perniola, Investigation of cyle-to-cycle variability in HfO_2-based OxRAM, IEEE Electron Dev Lett, vol. 37, pp. 721-723 (2016). DOI: 10.1109/LED.2016.2553370

[21] M. Bargallo Gonzalez, J. Martin-Martinez, M. Maestro, M. Acero, M. Nafría, F. Campabadal, Investigation of filamentary current fluctuations features in the high-resistance state of Ni/HfO_2-based RRAM, IEEE Trans Electron Dev, 63, pp. 3116-3122 (2016). DOI: 10.1109/TED.2016.2583924

[22] M. Suri, V. Parmar, Exploiting intrinsic variability of filamentary resistive memory for extreme learning machine architectures, IEEE Trans Nanotech, vol. 14, pp. 963-968 (2015). DOI**:** 10.1109/TNANO.2015.2441112

[23] A. Chen, Utilizing the variability of resistive random access memory to implement reconfigurable physical unclonable functions, IEEE Electron Dev Lett, vol. 36, 138-140 (2015). DOI**:** 10.1109/LED.2014.2385870

[24] F. Pan, V. Subramanian, Kinetic Monte Carlo simulation of resistive switching and filament growth in electrochemical RRAMs, Dev Res Conf (DRC), 2010. DOI**:** 10.1109/DRC.2010.5551973

[25] S. Aldana, P. García-Fernández, A. Rodríguez-Fernández, R. Romero-Zliz, M.B. González, F. Jiménez-Molinos, F. Campabadal, F. Gómez-Campos, J. Roldán, A 3D kinetic Monte Carlo simulation study of resistive switching process in $Ni/HfO_2/Si\text{-}n^+$-based RRAMs, J Phys D: Appl Phys, vol. 50, n. 33 (2015). DOI: 10.1088/1361-6463/aa7939

[26] Y. Li, M. Zhang, S. Long, J. Teng, Q. Liu, H. Lv, E. Miranda, J. Suñé, M. Liu, Investigation on the conductive filament growth dynamics in resistive switching memory via a universal Monte Carlo simulator, Sci Rep, vol. 7, 11204 (2017). DOI: 10.1038/s41598-017-11165-5

[27] A. Mehonic, M. Munde, W. Ng, M. Buckwell, L. Montesi, M. Bosman, A. Shluger, A.J. Kenyon, Intrinsic resistance switching in amorphous silicon oxide for high performance SiO_x ReRAM devices, Mic Rel, vol. 178, pp. 98-103 (2017). DOI: 10.1016/j.mee.2017.04.033

[28] E. Miranda, D. Jiménez, J. Suñé, The quantum point-contact memristor, IEEE Elec Dev Lett, vol. 33, pp. 1474-1476 (2012). DOI**:** 10.1109/LED.2012.2210185

[29] A. Avellán, E. Miranda, D. Schroeder, W. Krautschneider, Model for the voltage and temperature dependence of the soft breakdown current in ultrathin gate oxides, J Appl Phys, vol. 97, 014104 (2005). DOI: 10.1063/1.1827343

[30] E. Miranda, A. Mehonic, J. Blasco, J. Suñé, A.J. Kenyon, Multiple diode-like conduction in resistive switching SiO_x-based MIM devices, IEEE Trans Nanotech, vol. 14, pp. 14-17 (2015). DOI**:** 10.1109/TNANO.2014.2374232

[31] A. Belmonte, R. Degraeve, A. Fantini, W. Kim, M. Houssa, M. Jurczak, L. Goux, Origin of the deep reset and low variability of pulse-programmed W/Al2O3/TiW/Cu CBRAM device, IEEE 6th International Memory Workshop (IMW), 18-21 May 2014. DOI: 10.1109/IMW.2014.6849356

[32] F. Puglisi, L. Larcher, G. Bersuker, A. Padovani, P. Pavan, An empirical model for RRAM resistance in low-and high-resistance states, IEEE Electron Dev Lett, vol 34, pp. 387-389 (2013). DOI: 10.1109/LED.2013.2238883

[33] P. Brockwell and R. Davis, Introduction to time series and forecasting, 2002, Springer. ISBN: 978-0-387-95351-9

[34] V. Karpov, D. Niraula, Log-normal statistics in filamentary RRAM devices and related systems, IEEE Trans Electron Dev, vol. 38, pp. 1240-1243 (2017). DOI**:** 10.1109/LED.2017.2734961

[35] G. Box, M. Muller, A note on the generation of random normal deviates, Annals Math. Statistics, vol. 29, pp. 610-611, 1958. DOI: 10.1214/aoms/1177706645

[36] G. Patterson, J. Suñé, E. Miranda, Voltage-driven hysteresis model for resistive switching: SPICE modeling and circuit applications, IEEE Trans Comp-Aided Design Int Circ and Sistems, vol. 36, pp. 20144-2051, 2017. DOI: 10.1109/TCAD.2017.2756561